Chemical Engineering Journal 116 (2006) 163–172

Chemical Engineering Journal

www.elsevier.com/locate/cej

The effect of different feed flow patterns on the conversion of bubble column reactors

Everton Moraes Matos *, José Roberto Nunhez

Universidade Estadual de Campinas, UNICAMP, Faculdade de Engenharia Química, Departamento de Processos Químicos, C.P. 6066, Campinas, SP, CEP 13081-970, Brazil

Received 5 July 2005; received in revised form 9 November 2005; accepted 17 November 2005

Abstract

The main objective of this work is to improve the conversion inside bubble column reactors by varying the way in which feed is input inside these systems. Bubble column reactors are usually cylindrical in shape, and the reactor feed is at the bottom. The whole idea lies on the fact that the fluid dynamic fields inside the reactor affect its yield. Since the flow pattern in these reactors depend on the radial feed velocities profiles and radial feed holdup profiles at the bottom, several radial feed profiles for these variables were tested in order to analyze how they affect the reactor conversion. The mass flow input for both phases is the same in all situations. This in-house model uses an Eulerian–Eulerian approach to simulate a set of idealized radial profiles feed input situations, that will produce different fluid dynamic fields inside the reactor, and their effect on reactor conversion. The fluid dynamics and concentrations fields, for each phase, is estimated using mass and momentum conservation equations. Turbulence is taken into account using the k–ε model. The petroleum thermal hydrocraking is modeled using a pseudo-component model.

Keywords: Bubble column; Hydrocracking; Petroleum; Pseudo-componentes; k–ε model

1. Introduction

Bubble column reactors are widely used for hydrocracking process mainly because they provide a large contact area between gas and liquid phases and give a good temperature homogenization due to internal circulation. Hydrocracking consists in the hydrogenation of larger molecules turning them into lighter molecules of greater commercial value. Since the petroleum is composed by a large amount of different molecules, its behavior is modeled using pseudo-components [1].

Although Eulerian modeling is not an outstanding approach, no other available model using a different approach showed favorable for predicting bubble columns flow [2]. The contribution of this work is to explore different mode of operation for bubble column reactors, promoting different flow patterns for the phases inside and study their effects on reactor conversion, since fluid dynamic fields have great influence in flow regime transitions in bubble columns [3].

The geometry of the reactor is shown in Fig. 1. Since the geometry is symmetric, an axial symmetry two-dimensional model is used to represent the reactor. The characteristic reactor dimensions are reactor height and radius.

This work studies the way that the reactor feed affects the flow pattern inside the reactor. Therefore this work investigates how conversion can be affected by several different velocity profiles for the liquid feed as well as the gas fraction input inside the Bubble column reactor. The mass flow input is the same for all conditions.

The Navier–Stokes equations are the momentum conservation equations used to predict the velocity profile. The continuity equations are the mass conservation equations, which are used for the prediction of the volume fraction of the phases, the holdups [4]. The k–ε model is used to account for turbulence. A kinetic model based on pseudo-components represents the petrol.

The numerical method is the finite volume method. It uses the SIMPLEC algorithm for the velocity–pressure coupling [5].

2. Modeling

In order to represent the complex petroleum mixture, a model of six pseudo-components is used. The groups represented in

* Corresponding author. Tel.: +55 19 3788 3967; fax: +55 19 3788 3965.
E-mail addresses: evertonmm@uol.com.br (E.M. Matos), nunhez@feq.unicamp.br (J.R. Nunhez).

1385-8947/$ – see front matter © 2005 Elsevier B.V. All rights reserved.
doi:10.1016/j.cej.2005.11.004

Nomenclature

A_h	heavy aromatics
A_l	light aromatics
C_i	concentration of lump i (mol/cm^3)
C_m	constant of radial force
C_w	constant of interfacial drag force (kg/m^3 s)
D	dispersion coefficient for phase k (m^2/s)
E	roughness factor
g	gravitational constant (m^2/s)
k	turbulent kinetic energy (J/kg)
k_i	constant of reaction for path i (h^{-1})
N_h	heavy naphthenes
N_l	light naphthenes
P_h	heavy paraffins
P_l	light paraffins
r_i	rate of reaction for species i (kg/s)
r	radial position (m)
$u_{r,g}$	gas velocity, r-component (m/s)
$u_{z,g}$	gas velocity, z-component (m/s)
$u_{r,l}$	liquid velocity, r-component (m/s)
$u_{z,l}$	liquid velocity, z-component (m/s)
y	distance from the wall (m)
z	axial position (m)

Greek symbols

ε_{diss}	turbulence dissipation rate (J/kg s)
ε_g	gas holdup (m^3/m^3)
ε_l	liquid holdup (m^3/m^3)
$\mu_{eff,k}$	effective viscosity of phase k (kg/m s)
μ_k	viscosity of phase k (kg/m s)
$\mu_{t,k}$	turbulent viscosity of phase k (kg/m s)
$\nu_{t,k}$	kinematics turbulent viscosity of phase k (m^2/s)
ρ_g	gas density (kg/m^3)
ρ_l	liquid density (kg/m^3)

the model are the heavy and light aromatics, the heavy and light naphthenes and the heavy and light paraffins. The kinetic net for the hydro-cracking is shown in Fig. 1 [1].

2.1. Mass balance

The mass balance for a two-phase flow in cylindrical coordinates, considering that the mass movement is due to diffusion and convection and considering that the mass transfer between phases negligible, is given by the following equations

$$\frac{\partial}{\partial z}\left(D\frac{\partial(\rho_L\varepsilon_L)}{\partial z}\right)+\frac{1}{r}\frac{\partial}{\partial r}\left(Dr\frac{\partial(\rho_L\varepsilon_L)}{\partial r}\right)-\frac{\partial(u_{zL}\rho_L\varepsilon_L)}{\partial z}-\frac{1}{r}\frac{\partial(ru_{rL}\rho_L\varepsilon_L)}{\partial r}=0 \quad (1)$$

The mass conservation implies that the holdup for both phases is equal to one:

$$\varepsilon_L+\varepsilon_G=1 \quad (2)$$

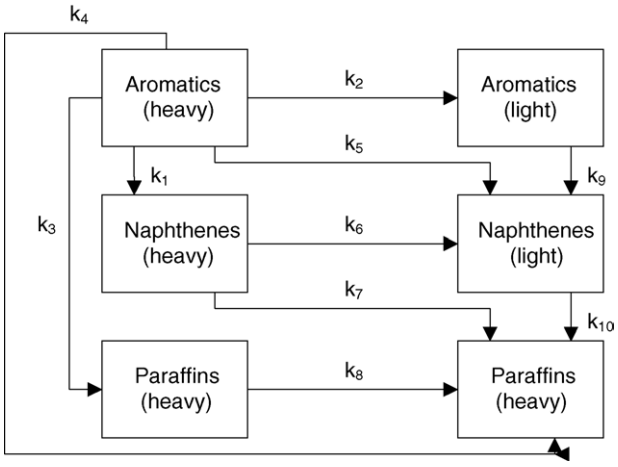

Fig. 1. Kinetic network.

The mass conservation for each species (pseudo-component) depends on the thermal reactions inside the kinetic net. The mass conservation for any species is given by

$$\frac{\partial}{\partial z}\left(D\varepsilon_L\frac{\partial C_A}{\partial z}\right)+\frac{1}{r}\frac{\partial}{\partial r}\left(Dr\varepsilon_L\frac{\partial C_A}{\partial r}\right)-\frac{\partial(u_{zL}\varepsilon_L C_A)}{\partial z}-\frac{1}{r}\frac{\partial(ru_{rL}\varepsilon_L C_A)}{\partial r}+r_A=0 \quad (3)$$

2.2. Momentum balance

The velocity of the fluid can be estimated trough a momentum balance, which includes a force balance in a cylindrical control volume. The stresses in a control volume are represented in Fig. 2.

The momentum balance is given by

$$\sum F=\frac{\partial(\text{mass}\cdot\text{velocity})}{\partial t} \quad (4)$$

That is to be applied in each direction.

The momentum conservation was applied for each phase in the axial and radial directions, which the friction terms considered [6]:

- For liquid in z direction:

$$2\frac{\partial[\varepsilon_L\mu_L(\partial u_{zL}/\partial z)]}{\partial z}+\frac{1}{r}\frac{\partial[\varepsilon_L r\mu_L(\partial u_{zL}/\partial r)]}{\partial r}+\frac{1}{r}\frac{\partial[\varepsilon_L r\mu_L(\partial u_{rL}/\partial z)]}{\partial r}-\frac{\partial(\varepsilon_L P)}{\partial z}+\varepsilon_L\rho_L g_z+C_W\varepsilon_G\varepsilon_L(u_{z,G}-u_{z,L})=\frac{\partial(\varepsilon_L\rho_L u_{ZL}^2)}{\partial z}+\frac{1}{r}\frac{\partial(\varepsilon_L\rho_L ru_{rL}u_{zL})}{\partial r}-N_{H_2}u_{zG} \quad (5)$$

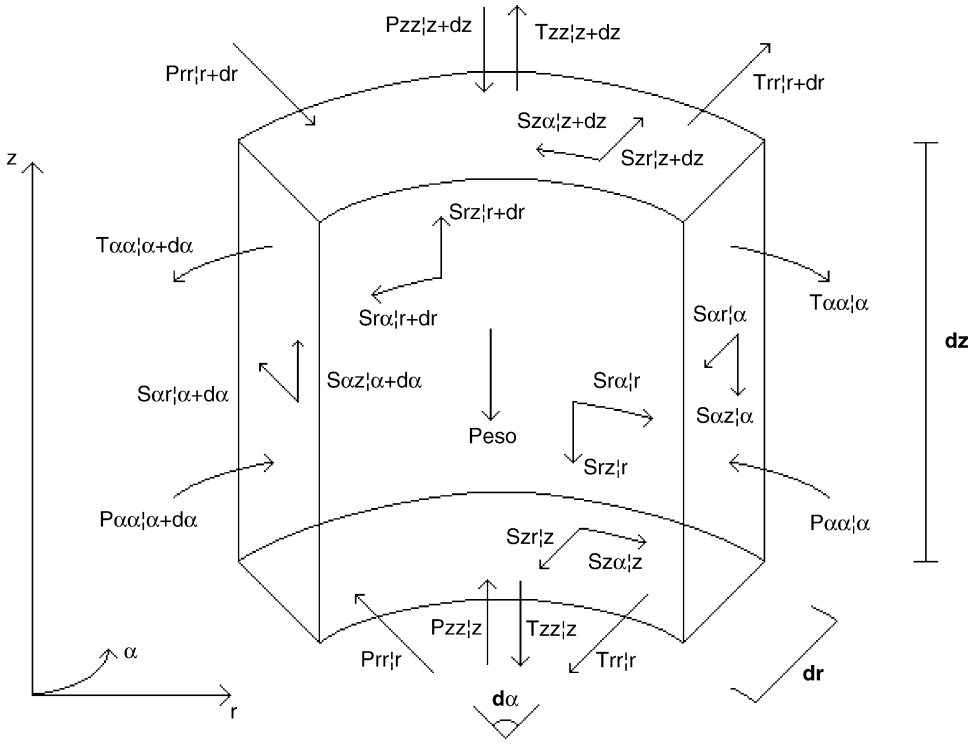

Fig. 2. Distribution of tensions in a cylindrical control volume.

- For gas in z direction:

$$2\frac{\partial[\varepsilon_G\mu_G(\partial u_{zG}/\partial z)]}{\partial z}+\frac{1}{r}\frac{\partial[\varepsilon_G r\mu_G(\partial u_{zG}/\partial r)]}{\partial r}+\frac{1}{r}\frac{\partial[\varepsilon_G r\mu_G(\partial u_{rG}/\partial z)]}{\partial r}-\frac{\partial(\varepsilon_G P)}{\partial z}+\varepsilon_G\rho_G g_z-C_W\varepsilon_G\varepsilon_L(u_{z,G}-u_{z,L})=\frac{\partial(\varepsilon_G\rho_G u_{ZG}^2)}{\partial z}+\frac{1}{r}\frac{\partial(\varepsilon_G\rho_G r u_{rG}u_{zG})}{\partial r}+N_{H_2}u_{zG} \quad (6)$$

- For liquid in r direction:

$$2\frac{1}{r}\frac{\partial[\varepsilon_L r\mu_L(\partial u_{rL}/\partial r)]}{\partial r}+\frac{\partial[\varepsilon_L\mu_L(\partial u_{zL}/\partial r)]}{\partial z}+\frac{\partial[\varepsilon_L\mu_L(\partial u_{rL}/\partial z)]}{\partial z}-2\mu_L\varepsilon_L\frac{u_{rL}}{r^2}-\frac{\partial(P\varepsilon_l)}{\partial r}+C_W\varepsilon_G\varepsilon_L(u_{r,G}-u_{r,L})-C_M\varepsilon_G\varepsilon_L\rho_L(u_{z,G}-u_{z,L})\frac{\partial u_{z,L}}{\partial r}=\frac{\partial(\varepsilon_L\rho_L u_{zL}u_{rL})}{\partial z}+\frac{1}{r}\frac{\partial(\varepsilon_L\rho_L r u_{rL}^2)}{\partial r}-N_{H_2}u_{rG} \quad (7)$$

- For gas in r direction:

$$2\frac{1}{r}\frac{\partial[\varepsilon_G r\mu_G(\partial u_{rG}/\partial r)]}{\partial r}+\frac{\partial[\varepsilon_G\mu_G(\partial u_{zG}/\partial r)]}{\partial z}+\frac{\partial[\varepsilon_G\mu_G(\partial u_{rG}/\partial z)]}{\partial z}-2\mu_G\varepsilon_G\frac{u_{rG}}{r^2}-\frac{\partial(P\varepsilon_g)}{\partial r}-C_W\varepsilon_G\varepsilon_L(u_{r,G}-u_{r,L})+C_M\varepsilon_G\varepsilon_L\rho_L(u_{z,G}-u_{z,L})\frac{\partial u_{z,L}}{\partial r}=\frac{\partial(\varepsilon_G\rho_G u_{zG}u_{rG})}{\partial z}+\frac{1}{r}\frac{\partial(\varepsilon_G\rho_G r u_{rG}^2)}{\partial r}+N_{H_2}u_{rG} \quad (8)$$

2.3. Turbulence

In order to account for turbulence, the k–ε model is used. The equations in cylindrical coordinates are [6]:

- Turbulent kinetic energy:

$$\frac{\partial}{\partial z}\left(D\rho_L\varepsilon_L\frac{\partial k_L}{\partial z}\right)+\frac{1}{r}\frac{\partial}{\partial r}\left(D\rho_L\varepsilon_L r\frac{\partial k_L}{\partial r}\right)-\frac{\partial(\rho_L u_{zL}\varepsilon_L k_L)}{\partial z}-\frac{1}{r}\frac{\partial(\rho_L u_{rL}\varepsilon_L r k_L)}{\partial r}+G_L\varepsilon_L-\rho_L\varepsilon_{diss,L}\varepsilon_L=0 \quad (9)$$

- Turbulent dissipation:

$$\frac{\partial(\rho\varepsilon u_z\varepsilon_{diss})}{\partial z}+\frac{1}{r}\frac{\partial(\rho\varepsilon r u_r\varepsilon_{diss})}{\partial r}-\frac{\partial}{\partial z}\left(\frac{\mu}{\sigma}\varepsilon\frac{\partial\varepsilon_{diss}}{\partial z}\right)_G-\frac{1}{r}\frac{\partial}{\partial r}\left(\frac{\mu}{\sigma}\varepsilon r\frac{\partial\varepsilon_{diss}}{\partial r}\right)=\frac{\varepsilon_{diss(L/G)}}{k_{L/G}}(1.44G-1.92\rho_{L/G}\varepsilon_{diss})\varepsilon \quad (10)$$

and

$$G = \mu \left\{ 2 \left[\left(\frac{\partial u_{r\mathrm{L}}}{\partial r} \right)^2 + \left(\frac{u_{r\mathrm{L}}}{r} \right)^2 + \left(\frac{\partial u_{z\mathrm{L}}}{\partial z} \right)^2 \right] + \left[\frac{\partial u_{r\mathrm{L}}}{\partial z} + \frac{\partial u_{z\mathrm{L}}}{\partial r} \right]^2 \right\} \quad (11)$$

The turbulent viscosities are given by

$$\mu_{\mathrm{turb.,L}} = 0.09 \rho_{\mathrm{L}} \frac{k_{\mathrm{L}}^2}{\varepsilon_{\mathrm{diss}}} \quad (12)$$

$$\mu_{\mathrm{turb,G}} = \mu_{\mathrm{turb,L}} \frac{\rho_{\mathrm{G}}}{\rho_{\mathrm{L}}} R_{\mathrm{p}}^2 \quad (13)$$

where

$$\mu = \mu_{\mathrm{lam}} + \mu_{\mathrm{turb}} \quad (14)$$

The k–ε model for turbulence [7] was initially developed for a one phase system, later this model was adapted for a two-phase flows. The coupling of the turbulent viscosity of both phases are given by Eq. (13) [6].

2.4. Feed input profiles

The first feed input profile to be analyzed has already been published in another work [6,8]. For this case, the liquid axial velocity is 0.01 m/s and the gas axial velocity is 0.08 m/s. The feed gas holdup is 0.27. The reactor is 4 m high and its diameter is 0.3 m.

Another feed input profiles, which are not flat profiles, will be tested. They will have the same mass flow rate for both phases as the first flat feed profile. Therefore, the velocity profiles of the new feed inputs, with constant holdup, need to respect the following conditions:

$$\int_0^R r u_{z,z=0}(r)\,\mathrm{d}r = \int_0^R r u^*_{z,z=0}(r)\,\mathrm{d}r \quad \text{with} \quad u^*_{z,z=0}(r) = 0.01\,\mathrm{m/s} \quad (15)$$

For non-flat holdup profiles with constant velocity:

$$\int_0^R r \varepsilon_{\mathrm{G}}(r)\,\mathrm{d}r = \int_0^R r \varepsilon^*_{\mathrm{G},z=0}(r)\,\mathrm{d}r \quad \text{with} \quad \varepsilon^*_{z=0}(r) = 0.27 \quad (16)$$

The reactor behavior for feed inputs with radial velocity profiles will also be analyzed.

2.5. Further model consideration

The equation used for the calculation of the holdup of the liquid or of the gas is obtained through the subtraction of the continuity equations of each phase and using Eq. (2).

The model of this work was discretized using the volume finite method in a rectangular and orthogonal mesh with 12 finite volumes in the radial and axial direction. The velocities are calculated in the edges of the control volumes and the scalar variables, such as pressure, concentration and holdup, are calculated in the middle of each control volume. The boundary conditions are introduced using fictitious control volumes.

In order to avoid negatives coefficients in the equations, which leads to numeric instability, it was used the upwind scheme to discretize the convective terms while the diffusion terms were discretized by central differences.

The model uses the SIMPLEC method [5].

The mass transport between the phases has not been considered. This consideration is based mainly on the covalent nature of the chemical components present in the mixture results in low reaction rates. It causes low gas consumption and the mass transfer between the phases is negligible in comparison to the transport rate by turbulent convection and diffusion.

The convergence criterion adopted, based on the pressure, is given by

$$\left| \sum_{j=2}^{13} \sum_{i=2}^{13} P_{ij}^{(n+1)} - \sum_{j=2}^{13} \sum_{i=2}^{13} P_{ij}^{(n)} \right| < 10^{-9} \quad (17)$$

It has been observed that, in turbulent flows, the momentum diffusivity is close to the mass diffusivity, i.e., the Schmidt number is close to unity [6]. This observation gives an important correlation for the estimation of the turbulent diffusion coefficient. In this case, the viscosity becomes a flow property and not anymore a fluid property and, thus, the diffusion coefficient (D) can be expressed by

$$Sc = \frac{\text{difusividade do momentum}}{\text{difusividade da massa}} = \frac{\mu/\rho}{D} \approx 1 \quad (18)$$

$$D = \frac{\mu}{\rho} \quad (19)$$

2.6. Boundary conditions

In this work, the velocity profiles and the holdup of both phases at the entrance of the reactor are not plain profiles such as those presented in previous works. The inlet radial velocities are not equal to zero in some cases. The boundary conditions at the entrance of the reactor for the turbulent variables of the k–ε model were modeled using the considerations of the work of Xu et al. [9]. The concentrations of the pseudo-components have a prescribed value at the inlet.

At the central line, the axial velocities, holdups, concentrations and the turbulent variables of the k–ε model have derivative equal to zero due to the axial symmetry consideration. For the same reason, the radial velocities are equal to zero at this boundary.

At the wall, the axial and radial velocities are equal to zero for both phases. The holdup has a derivative equal to zero at this boundary, since there is not diffusion through the wall. A wall function has also been employed in the model.

The wall functions to the k–ε model are [9]:

$$|u_{zL,wall}| = \frac{\sqrt{\tau_{w,k}/\rho_k}}{0.42} \ln\left[E\frac{\sqrt{\tau_{w,k}/\rho_L}}{\mu_L/\rho_L}y\right] \quad (20)$$

$$k_{sl} = \frac{(\tau_{w,sl}/\rho_l)^2}{\sqrt{0.09}} \quad (21)$$

$$\varepsilon_{d,sl} = \frac{(\tau_{w,sl}/\rho_l)^3}{0.42y} \quad (22)$$

First the wall stress is estimated by Eq. (20), and after, with wall stress value, the values of k and ε are estimated using Eqs. (21) and (22), respectively. The motivation for the use of wall functions is because in the development of the k–ε model, the Reynolds number do not assume near zero values near the walls. When the Reynolds number is low, wall functions are used instead of the k–ε model.

There is no axial velocity for the liquid phase at the free surface (flat surface). The holdups, radial velocities, concentrations and the turbulent variables, k and ε, are locally parabolic at the free surface (normal derivatives equal to zero). The liquid leaves the reactor through the upper part of the cylinder and the velocity at the outlet is calculated respecting the global mass conservation. Since the adsorption of gas by the liquid is negligible, the gas fraction must be constant in the axial direction (mass conservation).

Previous works indicate that the model needs to consider a friction factor varying with the radial coordinate. The friction factor, C_W, in general, has to depend upon the bubble size but this dependence is weak for 1–10 mm diameter bubbles [10]. The C_W value equal to 5×10^4 kg/m^3 s leads to a slip velocity between phases around 0.2 m/s, which agrees well with experimental observations [10]. This work follows the observations of Grienberger and Hofmann [6], that present for a better agreement with experimental values. The expression for the friction factor between the phases is given by a radial coordinate function, presented below:

$$C_W = 50\,000(2.2 - 1.7\sqrt{r/R}) \quad (23)$$

Table 1
Kinetic and fluid dynamics constants

Variable	Value
k_1 (h^{-1})	1.2633
k_4 (h^{-1})	0.6042
k_3 (h^{-1})	0.0421
k_4 (h^{-1})	0.5309
k_5 (h^{-1})	0.0397
k_6 (h^{-1})	1.1855
k_7 (h^{-1})	0.1619
k_8 (h^{-1})	0.4070
k_9 (h^{-1})	0.2909
k_{10} (h^{-1})	0.0818
C_W (kg/m^{3}s)	50000
C_M	−0.5
E	9.0

The radial friction factor, C_M, present in the Magnus force, is due to a bubble rotation that occurs when a rigid surface (in this case a gas bubble) moves in a non-uniform flow field. The non-uniform flow field may induce particle rotation, which causes an additional force in the radial direction [10].

The relaxation coefficients, in the beginning, were set to 10^{-3} for the four velocities; radial and axial for both phases. As the iterations develop, the relaxation coefficients were increased and they were close to the unity in the final solution. This procedure makes the processing time smaller.

The value considered for the gas density was an average between the value of this property at the base of the column (where the pressure is greater) and the value in the free surface under atmospheric pressure. This value remains constant because the gas phase is modeled as an incompressible fluid.

3. Results and discussions

The values for the parameters used in the model are presented in Table 1. The kinetic constants were taken from Krisna and Saxena [1] for a cut temperature of 700 °F (to distinguish heavy from light). The values for C_W and C_M were taken from Grienberger and Hofmann [6]. The other parameter values were set arbitrarily.

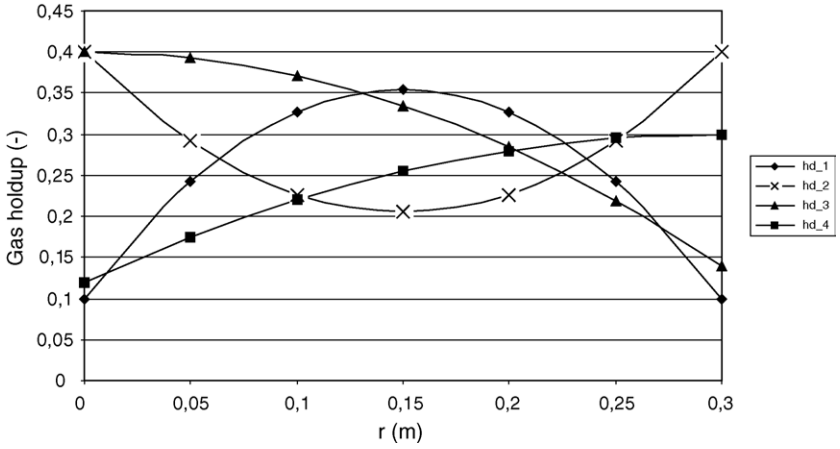

Fig. 3. Gas holdup input profiles.

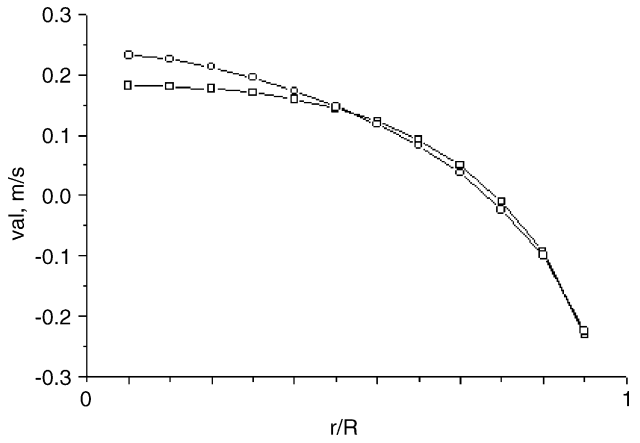

Fig. 4. Axial velocity of the liquid: val_1 (fist 1/3, □); val_2 (last 1/3, ◯); vag_sup ($z = 0$) = 0.08 m/s; gas holdup = 0.27.

The feed profiles presented were obtained with a liquid surface velocity of 0.01 m/s, a gas surface velocity of 0.08 m/s and volume fraction of gas of 27%. The internal radius is 0.3 m and the height of the reactor is 4.0 m. The initial concentration of heavy aromatics is 20 kg/m^3.

The feed profiles are presented in Fig. 3. The equations are given below:

$$\text{hd\_1} : \varepsilon_{G,z=0}(r) = -11.3333r^2 + 3.4r + 0.1 \quad (24)$$

$$\text{hd\_2} : \varepsilon_{G,z=0}(r) = 8.6666r^2 - 2.6r + 0.4 \quad (25)$$

$$\text{hd\_3} : \varepsilon_{G,z=0}(r) = -2.8888r^2 + 0.4 \quad (26)$$

$$\text{hd\_4} : \varepsilon_{G,z=0}(r) = -2r^2 + 1.2r + 0.12 \quad (27)$$

$$\text{vrl\_1} : u_{rL,z=0} = 2\,\text{m/s}$$

$$\text{vrl\_2} : u_{rL,z=0} = -2\,\text{m/s}$$

$$\text{vrl\_3} : u_{rL,z=0} = 1\,\text{m/s}$$

$$\text{vrl\_4} : u_{rL,z=0} = -1\,\text{m/s}$$

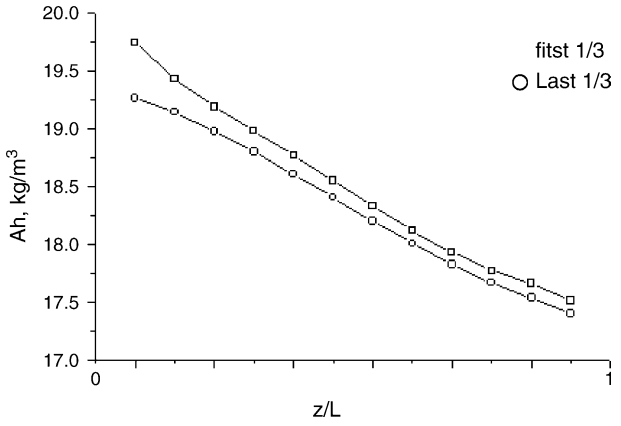

Fig. 5. Conversions to: val_1 (fist 1/3); val_2 (last 1/3); vag_sup ($z = 0$) = 0.08 m/s; gas holdup = 0.27.

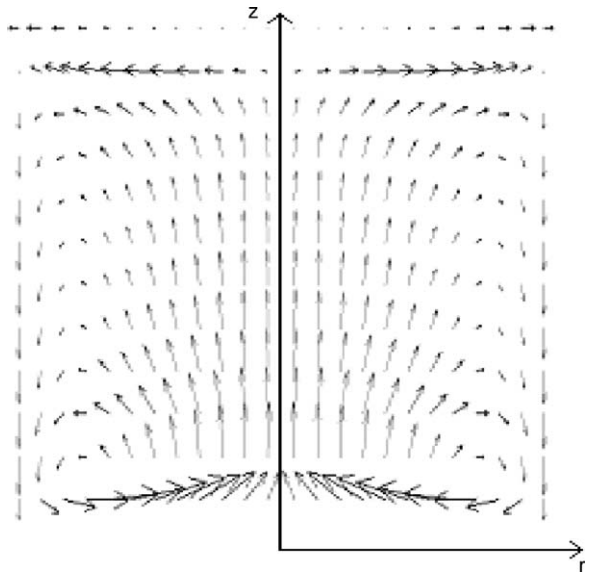

Fig. 6. Fluid dynamic field to hd_1; val_sup ($z = 0$) = 0.01 m/s; vag_sup ($z = 0$) = 0.08 m/s; gas holdup = 0.27.

val_1: all the inlet of the liquid fed until the first 1/3 of the radius.

val_2: all the inlet of the liquid fed after 2/3 of the radius.

In order to study the behavior of the chemical conversion associated to the different fluid dynamics profiles, the results due to Val_1 and Val_2 feed input profiles are shown in Fig. 4, which shows the axial velocities inside the reactor as a function of the reactor radius. Fig. 4 shows the results for liquid feed input in the first 1/3 of the reactor (Val_1—$0 < r < R/3$) and the last 1/3 of the radial length from the centerline (Val_2—$2R/3 < r < R$). The results indicate that the axial velocities around the centerline are higher when the liquid feed input is concentrated in the last 1/3 of the radius coordinate. Fig. 5 indicates that there is no significant difference for the conversion of heavy aromatic for

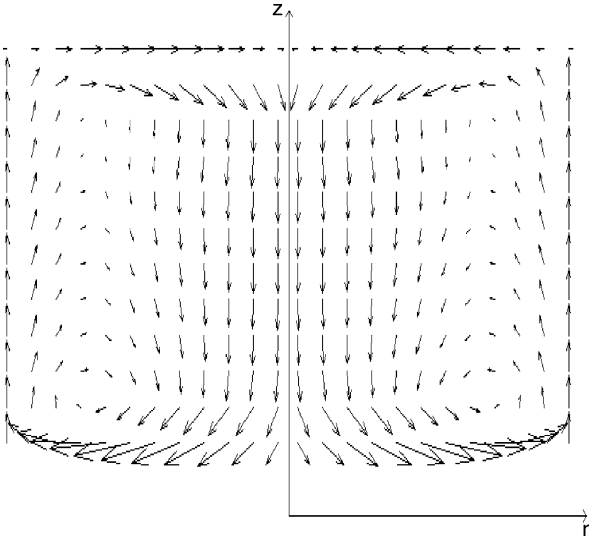

Fig. 7. Fluid dynamic field to hd_2; val_sup ($z = 0$) = 0.01 m/s; vag_sup ($z = 0$) = 0.08 m/s; gas holdup = 0.27.

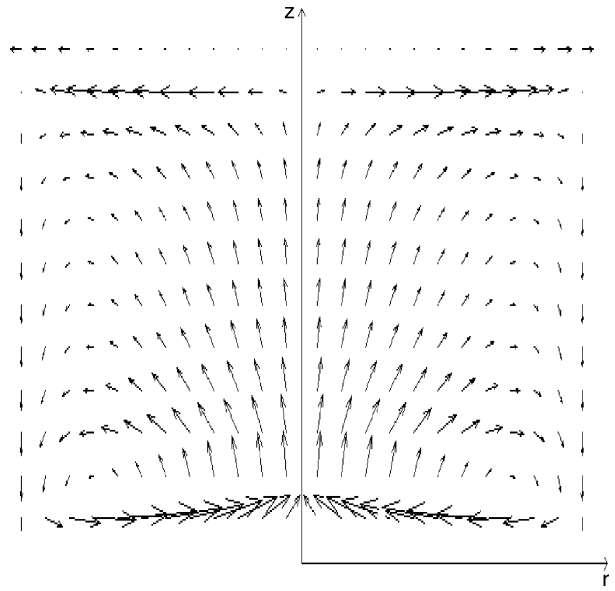

Fig. 8. Fluid dynamic field to hd_3; val_sup ($z = 0$) = 0.01 m/s; vag_sup ($z = 0$) = 0.08 m/s; gas holdup = 0.27.

the feed inputs Val_2 and Val_1. This indication gives an important information: since the yield is influenced by the reactor flow pattern, it is important to investigate which reactor flow pattern maximizes reactor yield.

Fig. 6 shows the velocity field of the liquid phase for the situation when the hd_1 profile (Eq. (24)) is adopted. When the gas holdup is higher at the centerline, the velocity field of liquid phase does not change considerably in comparison to the situation when the gas holdup is fed with uniform profile.

Fig. 7 shows the velocity field of the liquid phase for the situation when the hd_2 profile (Eq. (25)) is used. When the gas holdup is concentrated near the centerline and the wall, it is observed the inversion of the velocity field for the liquid phase in comparison to Fig. 6.

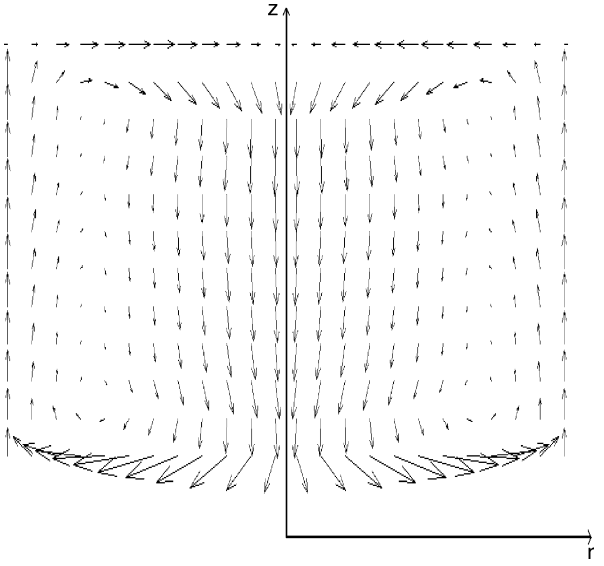

Fig. 9. Fluid dynamic field to hd_4; val_sup ($z = 0$) = 0.01 m/s; vag_sup ($z = 0$) = 0.08 m/s; gas holdup = 0.27.

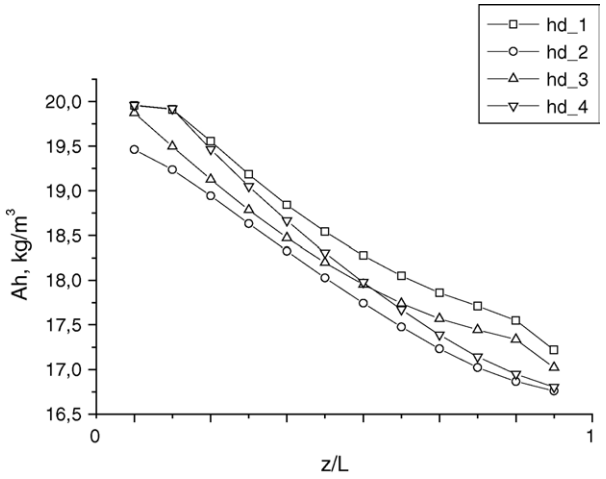

Fig. 10. Conversions associates to the hd_1 to hd_4.

Fig. 8 shows the velocity field of the liquid phase for the situation when the hd_3 profile (Eq. (26)) is used. When the gas holdup is higher near the centerline, the magnitude of the liquid axial velocity increases at the centerline, which improves the recirculation.

Fig. 9 shows the velocity field of the liquid phase for the situation when the hd_4 profile (Eq. (27)) is used. When the gas holdup is concentrated near the reactor wall, it can be observed that the liquid goes down in the centerline region and goes up near the wall.

Fig. 10 compares the heavy aromatic conversions along the axial coordinate as a function of the different feed input profiles. It was considered that the axial velocities for both phases are constant at the inlet. Only the inlet holdup profiles are not constant. Again, it has not been observed a considerable change

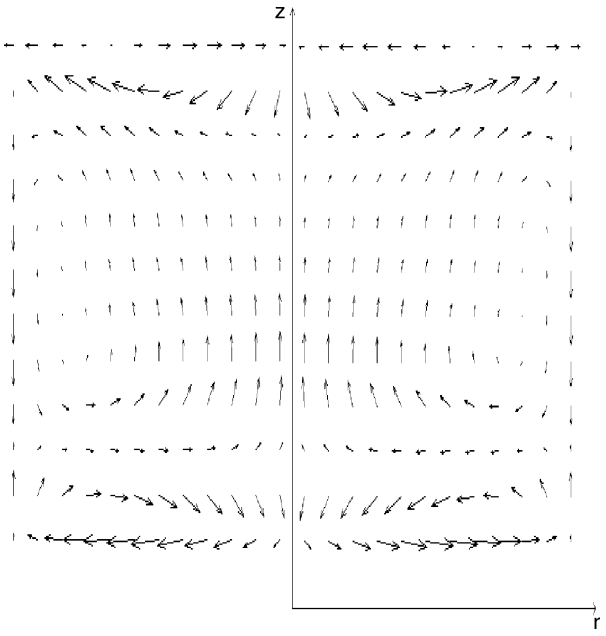

Fig. 11. Fluid dynamic field to vrl_1; val_sup ($z = 0$) = 0.01 m/s; vag_sup ($z = 0$) = 0.08 m/s; gas holdup = 0.27.

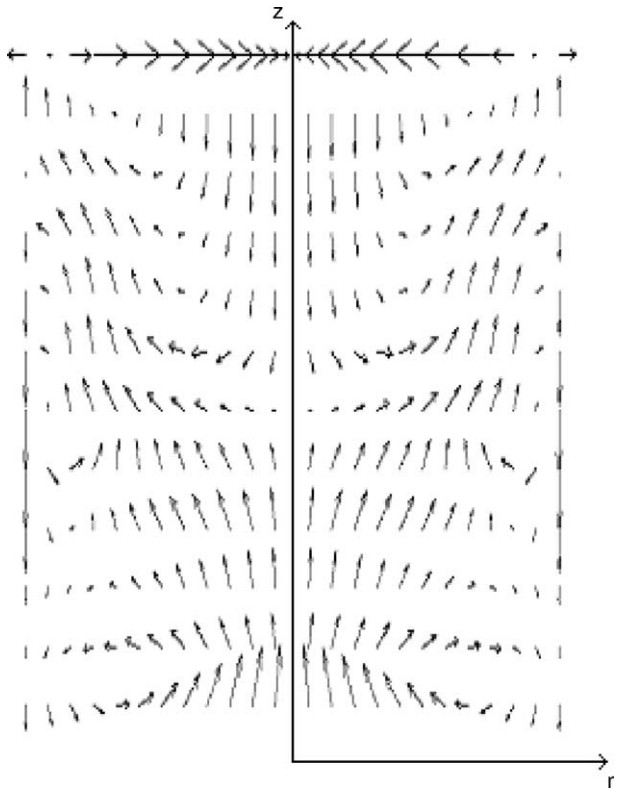

Fig. 12. Fluid dynamic field to vrl_2; val_sup ($z = 0$) = 0.01 m/s; vag_sup ($z = 0$) = 0.08 m/s; gas holdup = 0.27.

in the reactor conversion for the four non-uniform holdup profiles considered.

Fig. 11 shows the liquid velocity field when vrl_1 profile is used. It can be noticed an intense recirculation in the first and last 1/3 of the reactor height.

Fig. 12 presents the liquid velocity using the vrl_2 profile. A considerable recirculation can be observed near the wall.

Fig. 13 shows that the heavy aromatic conversions is somewhat similar for both cases.

Fig. 14 shows the liquid velocity field when vrl_3 profile is used. The recirculation was reduced because the magnitude of the axial liquid velocity at the centerline was enhanced by the radial liquid velocity input.

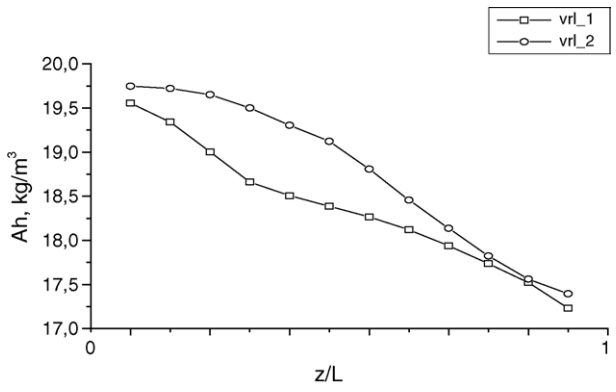

Fig. 13. Conversions associated to the vrl_1 and vrl_2 profiles.

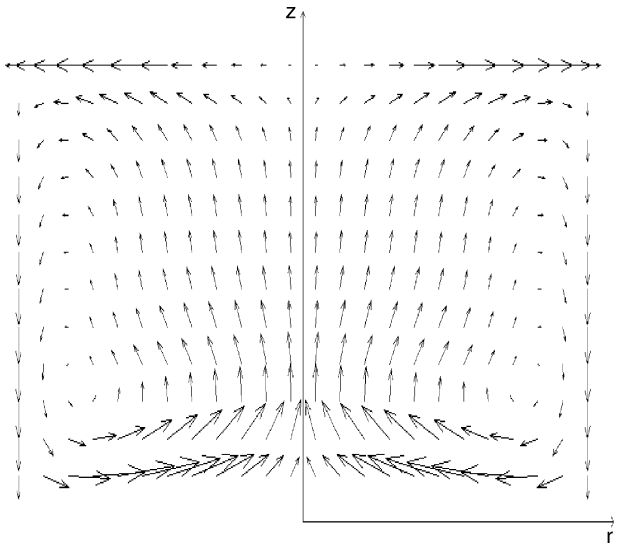

Fig. 14. Fluid dynamic field to vrl_3; val_sup ($z = 0$) = 0.01 m/s; vag_sup ($z = 0$) = 0.08 m/s; gas holdup = 0.27.

Fig. 15 presents the liquid velocity field when vrl_4 profile is adopted. It is observed that the recirculation was improved because the radial liquid velocity input intensified the magnitude of axial liquid velocity.

Fig. 16 compares the heavy aromatic conversions when the vrl_3 and vrl_4 are used. The results showed that the conversions do not change considerably at the reactor outlet.

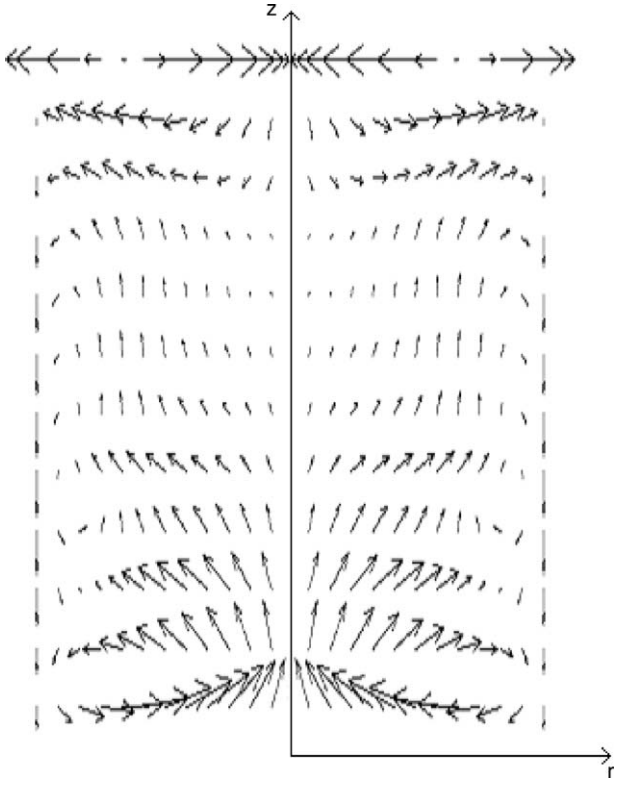

Fig. 15. Fluid dynamic field to vrl_4; val_sup ($z = 0$) = 0.01 m/s; vag_sup ($z = 0$) = 0.08 m/s; gas holdup = 0.27.

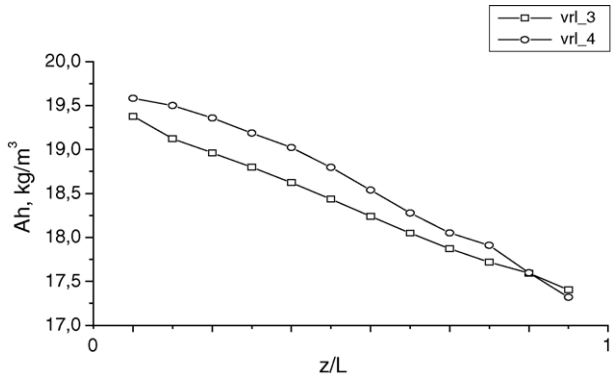

Fig. 16. Conversions associated to the vrl_3 and vrl_4 profiles.

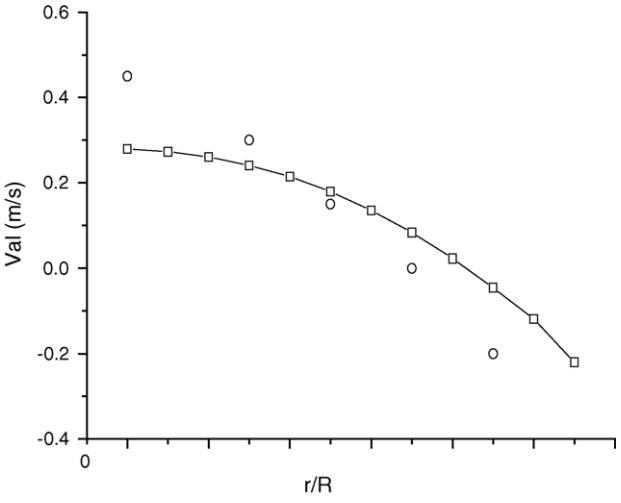

Fig. 17. Experimental comparison of the radial variation of the axial velocity of the liquid.

Fig. 17 compares the experimental and simulated values of the axial velocity of the liquid as a function of the radius and Fig. 18 compares the experimental and simulated gas holdup along the radius, for the same system considered in this work (Torvik, 1990). The experimental data were taken 2.5 m above the inlet.

The in-house model was developed using the C language for the computer code.

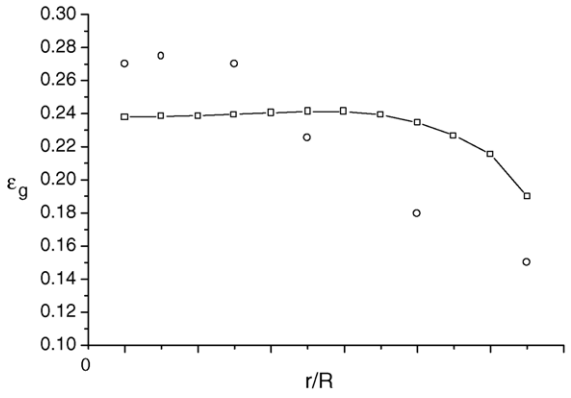

Fig. 18. Experimental comparison of the radial variation of the gas holdup.

4. Conclusions

The fluid dynamic model presented in this work simulates a set of idealized feed input situations which affects the flow fields, and their effect on the reactor conversion. Results indicate that the fluid dynamic fields inside the bubble column reactors do not affect considerably the reactor conversion. The model does not consider the influence of the bubble shape in the flow. Further refinements to the model could include this. Other turbulence models should also be tested in the model and this is also a future work. A comparison between the theoretical fluid dynamic fields, given by this work, and experimental flow fields for the simulated situations are not available in the literature and the same is true for the reactor conversion. This work realises that there is a need for more experimental research in this area. More realistic models for bubble columns reactors need improved models for the estimation of momentum transfer between phases and turbulence. The simplifications of this model however, do not limit important conclusions that can be drawn from this model, which was applied successfully, applicable to these type of reactors with good agreement with experimental data (Torvik, 1990). The new idea in this work is to show how different feed flow fields affect the conversion of bubble column reactors. Different field input profiles were used in order to obtain different flow fields. Figs. 4 and 5, for example, show that locating the feed of liquid in the region between the 2/3 of the radius and the wall improves recirculation and also yield.

Fig. 7 presents the velocity profile inside the reactor considering a parabolic profile with a concavity up for the gas holdup inlet. Fig. 9 presents the velocity profile for the case where the gas holdup is also a function of the radius in a parabolic profile. It can be noticed in both figures that there is an inverted flow inside the bubble column. The flow goes down near the reactor centerline and goes up next to the wall. The associated conversions to these profiles are presented in Fig. 10 and they suggest little differences in the associated chemical conversions.

Figs. 11 and 12 present the flow patterns when the feed has a prescribed value for the radial velocity of +2 m/s (in the direction of positive radius) and −2 m/s (in the direction of negative radius). Again, as showed in Fig. 13, little change has been observed in the chemical conversion. Figs. 14 and 15 shows the flow patterns for condition where there exist radial velocities in the feed and Fig. 16 shows the associated conversions.

Figs. 17 and 18 compare experimental and simulated profiles. The experimental results where extracted from Torvik and Svendsen [11].

This research indicates that conversion is not very much affected by the flow pattern inside bubble columns. However, since there are variations in the conversion depending on the reactor flow pattern, a deeper study including experimental validation could be done to see if it is worth modifying the feed input of petrochemical bubble column reactors.

Acknowledgment

The authors would like to thanks FAPESP for the grant received in this project.

References

[1] R. Krisna, K. Saxena, Use of an axial dispersion model for kinetic description of hydrocracking, Chem. Eng. Sci. 44 (3) (1989) 703–712.
[2] H.A. Jakobsen, H. Lindborg, C.A. Dorao, Modeling of bubble column reactors: progress and limitations, Ind. Eng. Chem. Res. 44 (2005) 5107–5151.
[3] T. Wang, J. Wang, Y. Jin, Theoretical prediction of flow regime transition in bubble columns by the population balance model, Chem. Eng. Sci. 60 (2005) 6199–6209.
[4] E.M. Matos, R. Guirardello, Modeling and simulation of a pseudo two-phase gas–liquid column reactor for thermal hydrocracking of petroleum heavy fractions, Brazil. J. Chem. Eng. 19 (3) (2002) 319–334.
[5] C.R. Maliska, Transferência de calor e Mecânica dos Fluidos Computacional, LTC, Rio de Janeiro, 1995.
[6] J. Grienberger, H. Hofmann, Investigations and modeling of bubble-columns, Chem. Eng. Sci. 47 (9–11) (1992) 2215–2220.
[7] B.E. Launder, D.B. Spalding, The numerical computation of turbulent flows, Comput. Meth. Appl. Mech. Eng. 3 (1974) 269–289.
[8] G. Hillmer, L. Weismantell, H. Hofmann, Investigations and modeling of slurry bubble columns, Chem. Eng. Sci. 49 (6) (1994) 837–843.
[9] Z.G. Xu, D.H.T. Gotham, M.W. Collins, J.E.R. Coney, C.G.W. Sheppard, S. Merdjani, Validation of turbulence models in a simulated air-conditioning unit, Int. J. Numer. Meth. Fluids 26 (1998) 199–215.
[10] A. Sokolichin, G. Eigenberger, Gas–liquid flow in bubble columns and loop reactors. Part I. Detailed modeling and numerical simulation, Chem. Eng. Sci. 49 (24B) (1994) 5735–5746.
[11] R. Torvik, H.F. Svendsen, Modeling of slurry reactors—a fundamental approach, Chem. Eng. Sci. 45 (8) (1990) 2325–2332.